

## Electrostatic Self-Assembly of Neutral and Polyelectrolyte Block Copolymers and Oppositely Charged Surfactant

Masahiko Annaka,\* Kanae Morishita, and Satoshi Okabe

Department of Chemistry, Kyushu University, Fukuoka 812-8581, Japan

Received: June 7, 2007; In Final Form: July 26, 2007

We investigated the phase behavior and the microscopic structure of the colloidal complexes constituted from neutral/polyelectrolyte diblock copolymers and oppositely charged surfactant by dynamic light scattering (DLS) and small-angle neutron scattering (SANS). The neutral block is poly(*N*-isopropylacrylamide) (PNIPAM), and the polyelectrolyte block is negatively charged poly(acrylic acid) (PAA). In aqueous solution with neutral pH, PAA behaves as a weak polyelectrolyte, whereas PNIPAM is neutral and in good-solvent condition at ambient temperature, but in poor-solvent condition above  $\sim 32$  °C. This block copolymer, PNIPAM-*b*-PAA with a narrow polydispersity, is studied in aqueous solution with an anionic surfactant, dodecyltrimethylammonium bromide (DTAB). For a low surfactant-to-polymer charge ratio  $Z$  lower than the critical value  $Z_C$ , the colloidal complexes are single DTAB micelles dressed by a few PNIPAM-*b*-PAA. Above  $Z_C$ , the colloidal complexes form a core-shell microstructure. The core of the complex consists of densely packed DTA<sup>+</sup> micelles, most likely connected between them by PAA blocks. The intermicellar distance of the DTA<sup>+</sup> micelles is  $\sim 39$  Å, which is independent of the charge ratio  $Z$  as well as the temperature. The corona of the complex is constituted from the thermosensitive PNIPAM. At lower temperature the macroscopic phase separation is hindered by the swollen PNIPAM chains. Above the critical temperature  $T_C$ , the PNIPAM corona collapses leading to hydrophobic aggregates of the colloidal complexes.

### Introduction

Interactions between polyelectrolytes and oppositely charged amphiphiles have attracted a great deal of interest in the last decades, due to their importance both in fundamental polymer physics/biophysics and in biological and industrial applications.<sup>1–5</sup> The interactions between polyelectrolytes and oppositely charged surfactants are quite strong and can induce a complex formation, often resulting in highly ordered structures. Both electrostatic interactions between the charged components and hydrophobic interactions between the polymer backbone and the alkyl chains of the surfactant are important in driving the self-assembly of molecules to form ordered structures. These well-defined supramolecular structures of the polyelectrolyte-surfactant complexes have unusual properties.

Stoichiometric polyelectrolyte-surfactant complexes usually precipitate from aqueous solution. However, Kabanov and co-workers<sup>6–9</sup> started to explore complexes formed by block polyelectrolyte and oppositely charged surfactants, in which the blocked segments could be either hydrophilic or hydrophobic. Therefore, this type of complex represents a special class of colloids that exhibit combined properties of amphiphilic copolymers and polyelectrolyte complexes. Colloidal complexes result from a self-assembly mechanism between polyelectrolyte-neutral block copolymer and oppositely charged surfactant. The block copolymer, also called double hydrophilic copolymer, is the key feature of the electrostatic self-assembly. The overall size and stability of the colloid depends on the nature of the electrostatic charges, on the molecular weight, and on the flexibility of the chains.

Recently, Berret and co-workers<sup>10–12</sup> have performed small-angle scattering (small-angle neutron scattering and small-angle X-ray scattering) studies of colloidal complexes resulting from the self-assembly of poly(acrylamide)-*block*-poly(sodium acrylate) as a neutral-anionic block copolymer and dodecyltrimethylammonium bromide as a cationic surfactant. They found that the complex exhibited a core-shell structure, of which the core is a dense and disordered microphase made of surfactant micelles connected by the polyelectrolyte blocks. The corona was a diffuse shell of the neutral chains and it ensured steric stability.

An interesting combination of a block copolymer is double-hydrophilic block copolymers in which one of the hydrophilic blocks is thermoresponsive, i.e., undergoes a transition from soluble to insoluble in water. When passing through the critical temperature, one of the hydrophilic blocks collapses, thus creating hydrophobic microdomains in analogy to polymeric surfactants. Or applying the thermal stimulus in the other direction, the aggregate formed by such block copolymers is dissociated. Poly(*N*-isopropylacrylamide) (PNIPAM) is well-known for its thermosensitive properties, exhibiting lower critical solution temperature (LCST) type phase behavior in water: at room temperature PNIPAM is hydrophilic and exists as individual random coil chains in water, while above  $\sim 32$  °C, PNIPAM becomes hydrophobic and collapses into a molecular globule.

In the present paper, we investigate the structure and the stability of colloidal complex made from poly(*N*-isopropylacrylamide)-*block*-poly(acrylic acid) (PNIPAM-*b*-PAA) (Figure 1) as thermosensitive neutral-anionic block copolymer and dodecyltrimethylammonium bromide (DTAB) as cationic surfactant under various conditions, specifically the effects of the DTAB

\* To whom correspondence should be addressed. Phone: +81-92-642-2594. Fax: +81-92-642-2607. E-mail: annaka-scc@mbox.nc.kyushu-u.ac.jp.

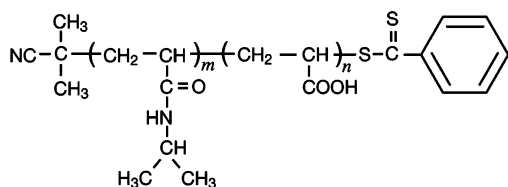


Figure 1. Chemical structure of PNIPAM-*b*-PAA.

concentration (surfactant-to-polymer charge ratio), addition of salt and temperature.

## Experimental Section

**Materials.** *N*-Isopropylacrylamide (NIPAM) was kindly supplied by KOHJIN and recrystallized from a toluene/hexane mixture and dried in vacuo. Acrylic acid (AA, Wako Pure Chemicals) was distilled under reduced pressure prior to use. 2,2'-Azobisisobutyronitrile (AIBN, Wako Pure Chemicals) was recrystallized from methanol. Benzene (Wako Pure Chemicals) and methanol (Wako Pure Chemicals) were distilled over drying agent under dry nitrogen atmosphere prior to use. A RAFT agent, 2-cyanopropylidithiobenzoate (CPDB), was prepared according to literature procedure.<sup>13–15</sup>

**Preparation of PNIPAM-*b*-PAA.** PNIPAM was prepared by reversible addition–fragmentation chain transfer (RAFT) polymerization with CPDB as a chain transfer agent (CTA). NIPAM, CPDB, and AIBN as initiator were dissolved in benzene. The solution was deoxygenated by 3 freeze–pump–thaw cycles, and polymerization was carried out at 70 °C for 14 h. The polymer was isolated by precipitation in an excess of diethyl ether, and purified by repeated precipitations, followed by drying in vacuo. RAFT polymerization of the diblock copolymers, PNIPAM-*b*-PAA, was performed with PNIPAM as the macro-CTA. Acrylic acid (AA), AIBN, and PNIPAM were dissolved in methanol, solutions were deoxygenated by 3 freeze–pump–thaw cycles, and polymerization was carried out at 67 °C. After polymerization, polymers were precipitated in an excess of diethyl ether and then dried in vacuo.

**Characterization.** *Gel Permeation Chromatography (GPC).* Both DMF and water were used as solvents for GPC to determine the molecular weight distribution of PNIPAM (macro-CTA) and PNIPAM-*b*-PAA. GPC of DMF-soluble PNIPAM was performed with a TOSOH HLC-8220GPC apparatus with TSKgel Super HM-Mx 2 columns, and in HPLC grade DMF with 10 mM LiBr was used as the mobile phase at a flow rate 0.4 mL/min at 40 °C. GPC using 50 mM NaHCO<sub>3</sub>/100 mM NaNO<sub>3</sub>/20 mM triethanol amine/0.03% NaN<sub>3</sub> was conducted on TSKgel G2500PW<sub>XL</sub> + G5000PW<sub>XL</sub> columns at a flow rate of 1.0 mL/min and 15 °C. Monodisperse poly(ethylene glycol) standards was used for calibration.

<sup>1</sup>H NMR. The number average molecular weight, *M<sub>n</sub>*, of PNIPAM (macro-CTA) was determined by <sup>1</sup>H NMR spectra, using a JEOL JNMAL300 spectrometer operating at a frequency of 300 MHz in CDCl<sub>3</sub>. The probe temperature was kept constant at ± 0.5 °C by the passage of thermostatically regulated air during accumulation. The temperature was measured with a calibrated thermocouple. The number-averaged molecular weight is estimated by comparing the <sup>1</sup>H NMR peak area of phenyl protons in the terminal dithiobenzoate with that of methine protons of PNIPAM side chains.

*Potentiometric Titration.* Potentiometric titration was carried out to determine the number average molecular weight of the PAA block in a titration vessel in which the temperature was controlled to within ± 0.1 °C of 25 °C under a nitrogen

atmosphere. Titration of PNIPAM-*b*-PAA in its acidic form was carried out with 200 mM NaOH aqueous solution as a titrant at 0.2 wt % polymer concentration, and the solution pH was monitored with a ORION 720A pH meter with ORION 8102BN electrode precalibrated with pH 4.01, 7.0, and 10 buffers. The titration was carried out slowly for several hours to allow for proper equilibration.

**Laser Light Scattering.** Static and dynamic light scattering (DLS) experiments were conducted with an ALV DLS/SLS-5000 light scattering system equipped with an ALV-5000 multiple  $\tau$  digital correlator for the measurements of the Rayleigh ratio  $R_\theta(q, c)$  and the collective diffusion coefficient  $D(c)$ . The wavevector  $q$  is defined as  $q = (4n\pi/\lambda) \sin(\theta/2)$ , where  $n$  is the refractive index of the solution,  $\lambda$  the wavelength of the incident beam ( $\lambda = 632.8$  nm), and  $\theta$  the scattering angle.

The excess Rayleigh ratio (eq 1) was determined from the scattering intensity at wavevector  $q = 1.87 \times 10^{-3} \text{ \AA}^{-1}$  ( $\theta = 90^\circ$ ) normalized with respect to that of benzene

$$\Delta R_\theta = \frac{I - I_0}{I_{\text{Ben}}} \left( \frac{n^2}{n_{\text{Ben}}^2} \right) R_{\text{Ben}, \theta} \quad (1)$$

where  $R_{\text{Ben}, \theta}$  is the Rayleigh ratio of benzene at scattering angle  $\theta$ , with the value of  $8.51 \times 10^{-6} \text{ cm}^{-1}$  at 632.8 nm;  $I$ ,  $I_0$ , and  $I_{\text{Ben}}$  are the scattered intensities of the solution, the solvent, and benzene, respectively; and  $n_{\text{Ben}}$  is the refractive index of benzene.

The autocorrelation functions were analyzed by performing the inverse Laplace transform, using the routine CONTIN assuming the superposition of exponentials for the distribution of relaxation times. The decay rate  $\Gamma$  of each process is calculated as the inverse of its relaxation time  $1/\Gamma$ . In the case of diffusive process, its diffusion coefficient  $D$  is obtained from the slope of  $\Gamma$  vs  $q^2$  by  $\Gamma = Dq^2$ . From this value the hydrodynamic radius was calculated according to the Stokes–Einstein equation:

$$R_H = \frac{k_B T}{6\pi\eta_0 D} \quad (2)$$

where  $k_B$  is the Boltzmann constant,  $\eta_0$  is the viscosity of the solvent, and  $T$  is the temperature of the sample. The polymer solutions were clarified by filtering through a Millipore membrane (0.45 mm pore size). The samples were equilibrated at each measurement temperature for at least 1 h.

**Small-Angle Neutron Scattering.** The small-angle neutron scattering (SANS) experiments were carried out at the SANS-U, Institute for Solid State Physics, University of Tokyo, installed at the research reactor JRR-3 at JAEA, Tokai, Japan.<sup>16</sup> Cold neutrons from the reactor, monochromatized with a velocity selector to a flux of neutrons with the wavelength of  $\lambda = 7 \text{ \AA}$  and its distribution of  $\Delta\lambda/\lambda = 0.1$ , were used as the incident beam. Each sample was put into a quartz cell with an optical length of 2 mm. The observed scattered intensity was corrected for cell and solvent scattering, incoherent scattering, and transmission and then rescaled to the absolute intensity, and then azimuthally averaged. The incoherent scattering from a polyethylene standard sample was used for the absolute intensity calibration. We recall that the expression of the intensity scattered by a dispersion of spherical and homogeneous particles of volume  $V$  and radius  $R$  is

$$\frac{d\sigma}{d\Omega}(q, c) = n(c)V^2 \Delta\rho^2 S(q, c) F(q, R) \quad (3)$$

**TABLE 1: Molecular Weight ( $M_w$ ), Molar Volume ( $V_{mol}$ ), Molecular Volume ( $v_0$ ), Coherent Neutron Scattering Length ( $b_N$ ), and Length Density ( $\rho_N$ ) of the Surfactant and the Polymers Studied in This Work<sup>16,17</sup>**

species	$M_w$ / g mol <sup>-1</sup>	$V_{mol}$ / cm <sup>3</sup> mol <sup>-1</sup>	$v_0$ / Å <sup>3</sup>	$b_N$ / 10 <sup>-12</sup> cm	$\rho_N$ / 10 <sup>10</sup> cm <sup>-2</sup>
<i>N</i> -isopropyl- acrylamide	113.16	128.9	214.1	1.336	0.711
acrylic acid	72.06	47.8	79.4	1.66	2.09
sodium acrylate	94.04	33	54.8	2.40	4.37
DTAB	308.35	495.5	495.5	-1.138	-0.23
DTA <sup>+</sup>	228.45	456.2	456.2	-1.817	-0.40
Br <sup>-</sup> *	79.9	39.3	39.3	0.679	1.73
D <sub>2</sub> O	20.02	18.0	30	1.92	6.38

**TABLE 2: Characterization of PNIPAM and Diblock Copolymers**

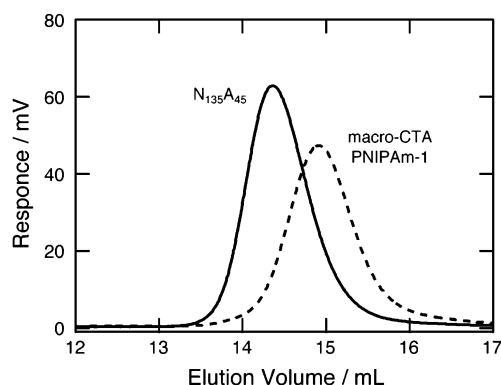
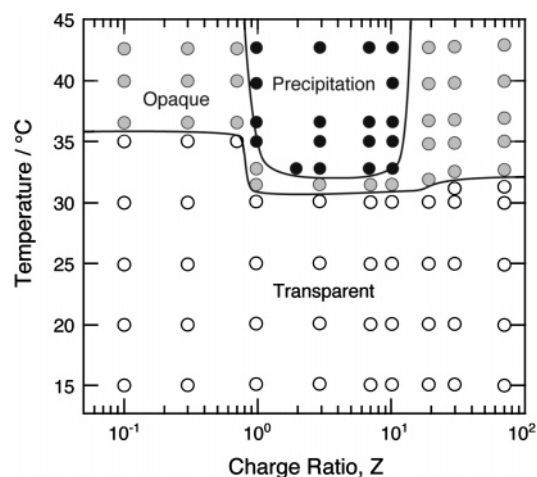
code	feed [M]/[CTA]/[I]	reaction time/h	$M_n$	monomer units [NIPAm]/[AAc]	PDI
PNIPAM-1	2000/10/2	11	13 500	118/-	1.15
PNIPAM-2	2000/10/2	14	15 500	135/-	1.16
PNIPAM-3	2000/10/2	22	20 000	175/-	1.18
N <sub>135</sub> A <sub>161</sub>	5000/10/2	12	27 500	135/161	—
N <sub>135</sub> A <sub>114</sub>	5000/10/2	6	24 100	135/114	1.18
N <sub>135</sub> A <sub>45</sub>	2000/10/2	4	18 700	135/45	1.14
N <sub>175</sub> A <sub>56</sub>	2000/10/2	4	24 200	175/56	1.28

where  $n(c)$  is the number density of particles at concentration  $c$ , and  $\Delta\rho (= \rho_N - \rho_S)$  is the difference of the scattering length density with respect to the solvent. Here,  $\rho_N$  and  $\rho_S$  are the scattering length density of the chemical species and the solvent, respectively.  $F(q)$  and  $S(q, c)$  are the form factor and the structure factor of the particles, respectively.

The coherent neutron scattering length densities for *N*-isopropylacrylamide, sodium acrylate, and DTAB are  $0.711 \times 10^{10}$ ,  $4.37 \times 10^{10}$ , and  $-0.23 \times 10^{10}$  cm<sup>-2</sup>, respectively. Therefore, in D<sub>2</sub>O ( $\rho_S = 6.38 \times 10^{10}$  cm<sup>-2</sup>) all these components are contributing to the total cross section. Lists of the coherent scattering lengths, molecular volumes, and coherent scattering length densities of the chemical species studied in this work are given in Table 1.<sup>17,18</sup>

## Results and Discussion

**Preparation and Characterization of Block Copolymer.** PNIPAM-*b*-PAA ( $N_m A_n$ , where  $m$  and  $n$  represent the number of NIPAM and acrylic acid units, respectively) was prepared by the RAFT process, and the block copolymerization was performed by using PNIPAM as a macromolecular chain transfer agent (macro-CTA). The molecular characteristics of the macro-CTA and the block copolymers, as they have been determined by <sup>1</sup>H NMR, GPC, and potentiometric titration, are presented in Table 2. [M], [CTA], and [I] indicate concentrations of monomer, macro-CTA (RAFT agent), and initiator, respectively. The obtained polydispersities are low. The living/controlled character of the polymerization is supported by the appearance of the characteristic UV signal at 500 nm due to the absorbance of the dithiobenzoate  $-S(C=S)-$  chromophore of the CTA for macro-CTAs and block copolymers. Another evidence of this feature is given by characteristic <sup>1</sup>H NMR signals for both the dithiocarbenzoate and 2-cyanopropyl end groups of the polymer. The use of CPDB leads to the formation of  $\omega$ -dithiobenzoate homopolymers. These are subsequently utilized as macro-CTAs in order to prepare diblock copolymers. The representative GPC trace of the PNIPAM-*b*-PAA clearly shows the formation of block copolymer: GPC trace shifts to the higher molecular weight region after polymerization of acrylic acid from PNIPAM macro-CTA (Figure 2). This indicates that the PNIPAM

**Figure 2.** GPC trace for macro-CTA (PNIPAM-1) and N<sub>135</sub>A<sub>45</sub> in 50 mM NaHCO<sub>3</sub>/100 mM NaNO<sub>3</sub>/20 mM triethanol amine/0.03% NaN<sub>3</sub> measured at 15 °C.**Figure 3.** Phase diagram obtained for the system of N<sub>135</sub>A<sub>45</sub>/DTAB/water at  $c = 0.4$  wt % with the degree of neutralization of PAA block  $\alpha = 0.75$ .

precursor efficiently participates as a macro-CTA via RAFT, therefore well-defined AB-type block copolymers are produced. In this study, we investigated the sample, coded as N<sub>135</sub>A<sub>45</sub>.

**Phase Behavior.** Polymer–surfactant phase diagrams were determined experimentally in a polymer–surfactant charge ratio  $Z$  range between 0.1 and 100 as a function of temperature at the desired concentration  $c$ . Here  $c$  is the total concentration defined as  $c = c_P + c_S$ , where  $c_P$  and  $c_S$  are the weight concentrations of polymer and of surfactant, respectively.  $Z$  is defined as  $Z = [S]/\alpha n[P]$ , where  $[S]$  and  $[P]$  are the molar concentrations for the surfactant and for the polymer, respectively.  $\alpha$  and  $n$  denote the degree of neutralization and the average number of monomers in the polyelectrolyte block, respectively.  $Z = 1$  describes the isoelectric solution, characterized by the same number densities of positive (DTA<sup>+</sup>) and negative (COO<sup>-</sup>) charged ions. The ( $Z, T$ )-phase diagram obtained for the system N<sub>135</sub>A<sub>45</sub>/DTAB/water at  $c = 0.4$  wt %,  $\alpha = 0.75$  is displayed in Figure 3. The data points in Figure 3 were obtained from light scattering experiments by measuring 90° scattering intensity, and by direct visualization. We distinguish macroscopically three regions in the phase diagram: homogeneous and transparent solution, opaque solution, and precipitation. At lower temperature, the solutions remain clear regardless of the charge ratio  $Z$ . The PNIPAM chains stabilize the complex formed between PAA block and DTAB, probably in the form of a core-corona particle. With increasing temperature, the aqueous mixtures turn slightly turbid at 32–35 °C depending on the charge ratio  $Z$ . The PNIPAM chains



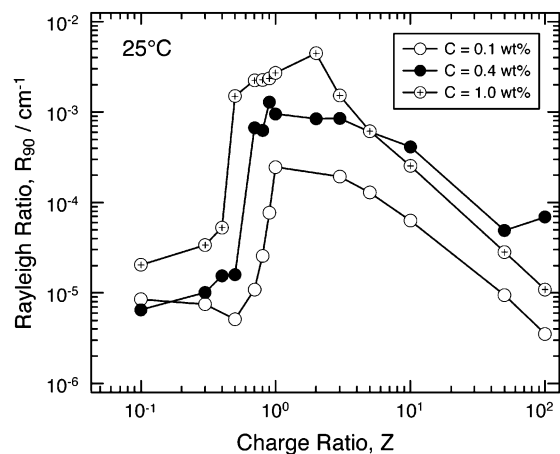


**Figure 4.** Rayleigh ratio measured for aqueous solutions of  $N_{135}A_{45}$ /DTAB at  $c = 0.1, 0.4$ , and  $1.0$  wt % with the degree of neutralization of PAA block  $\alpha = 0.75$  at  $25$  °C. The experiments are performed at  $q = 1.87 \times 10^{-3} \text{ \AA}^{-1}$  ( $\theta = 90^\circ$ ).

start to collapse and the collapsed PNIPAM globules may have a tendency to form hydrophobic aggregates. For the charge ratio  $Z$  between  $1.0$  and  $10$ , there exists a critical temperature  $T_C$  above which two phases coexist. Under the isoelectric condition at  $Z = 1$ , the complex is practically uncharged due to the electrostatic binding of DTAB, which allows the LCST-type phase separation of the PNIPAM blocks at higher temperature. Above  $Z = 10$ , a redissolution of precipitated large complexes takes place. When a large excess of DTAB is added to the  $N_{135}A_{45}$ /DTAB/water system, electrostatic intercomplex repulsion induced by the binding of DTAB micelles to hydrophobic aggregates may lead to a redissolution of precipitates. The system under investigation is a four-component system, including polyelectrolyte, simple salt, surfactant, and complex salt, therefore the full description of the phase diagram with tie lines and lever rules is more complex than the one displayed in Figure 3.

**Critical Charge Ratio for the Complex Formation.** For the light scattering experiments,  $N_{135}A_{45}$ /DTAB solutions with the degree of neutralization  $\alpha = 0.75$  were prepared in  $H_2O$  at total concentrations  $c = 0.1, 0.4$ , and  $1.0$  wt % with  $Z$  comprised between  $0.1$  and  $10$ . The Rayleigh ratios measured at  $q = 1.87 \times 10^{-3} \text{ \AA}^{-1}$  ( $\theta = 90^\circ$ ) for those three concentrations are shown in Figure 4. At low values of  $Z$ , the scattering intensity is independent of surfactant concentration and it remains at the level of the pure polymer ( $Z = 0$ ). With increasing  $Z$ , there exists a critical charge ratio noted  $Z_C$ , and comprised between  $0.5$  and  $1.0$  depending on the polymer concentration, above which the Rayleigh ratio increases by several orders of magnitude, indicating the formation of colloidal complexes. The Rayleigh ratio then decreases slowly at higher  $Z$  values. At large  $Z$ , the DTAB is in excess with respect to polymer, therefore all the polymers are consumed to form the colloidal complexes. Since the polymer concentration decreases with  $Z$  according to  $c_p = c/(1 + \alpha nZ)$ , the number of colloidal complexes and thus the scattering intensity decreases.

Figure 5 shows the normalized intensity autocorrelation functions of a  $0.4$  wt %  $N_{135}A_{45}$  solution for degree of neutralization  $\alpha = 0.75$  at  $q = 1.87 \times 10^{-3} \text{ \AA}^{-1}$  with various  $Z$  values at  $25$  °C. The distributions of relaxation times are shown in the inset. The observed behaviors are almost identical with those obtained for  $c = 0.1$  and  $1.0$  wt % (not shown). At  $Z = 0.1$ , two relaxation processes are observed. The fast process with diffusivity  $D_{\text{fast}} = 3.4 \times 10^{-7} \text{ cm}^2/\text{s}$ , which corresponds to a hydrodynamic radius  $R_{H,\text{fast}} = 55 \pm 1.1 \text{ \AA}$ , is attributed to a

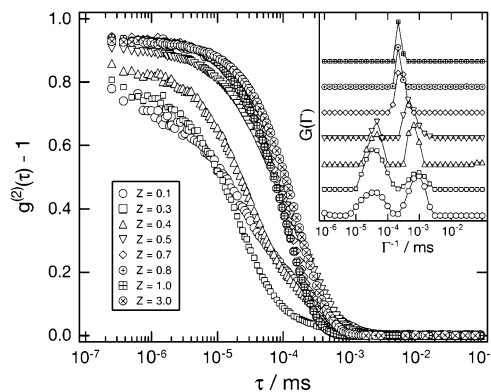


**Figure 5.** The normalized intensity autocorrelation functions of a  $0.4$  wt %  $N_{135}A_{45}$ /DTAB aqueous solution for degree of neutralization  $\alpha = 0.75$  at  $q = 1.87 \times 10^{-3} \text{ \AA}^{-1}$  with various  $Z$  values ranging from  $0.1$  to  $3.0$  at  $25$  °C. The relaxation time distributions are shown on the inset for the respective  $Z$  values.

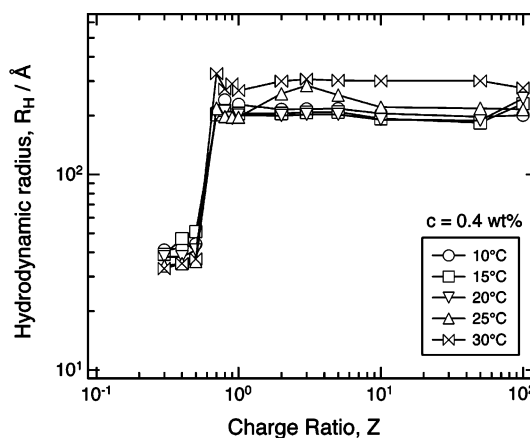


**Figure 6.** The evolution of the hydrodynamic radius  $R_H$  for a  $0.4$  wt %  $N_{135}A_{45}$ /DTAB aqueous solution with the degree of neutralization  $\alpha = 0.75$  on the whole range of  $Z$  values at various temperatures.

single polymer chain, while a slower process with diffusivity  $D_{\text{slow}} = 0.19 \times 10^{-7} \text{ cm}^2/\text{s}$ , which corresponds to a hydrodynamic radius  $R_{H,\text{slow}} = 969 \pm 25 \text{ \AA}$ , is also observed. This process may be attributed to some kind of polymer aggregation. Both processes exhibit low scattering intensities; this is expected for the unimer chains due to their small size, whereas for the polymer aggregates, it suggests that they are either very few in number or highly hydrated and, therefore, have a low scattering contrast. It is worthy to mention that since the CONTIN analysis renders the intensity-weighted distribution, the proportion of the large particle is strongly exaggerated, as the scattering intensity is dependent on the particle radius ( $\sim R^6$  for spherical particle). The formation of these aggregates is still not well understood. The observed behavior is almost identical with those up to  $Z = 0.5$ . Above  $Z = 0.7$ , a remarkable change in the relaxation process is observed as shown in Figure 5. Here the normalized intensity autocorrelation function exhibits a single-exponential function with diffusive character of the concentration fluctuations. The diffusion coefficient  $D = 0.9 \times 10^{-7} \text{ cm}^2/\text{s}$  corresponds to hydrodynamic radius  $R_H = 207 \pm 5 \text{ \AA}$ . It is interesting to note that the polydispersity is narrower than that of a single diblock copolymer chain.

Figure 6 exhibits the evolution of the hydrodynamic radius  $R_H$  for a  $0.4$  wt %  $N_{135}A_{45}$ /DTAB solution for degree of neutralization  $\alpha = 0.75$  on the whole range of  $Z$  values at various temperatures. Three scattering regimes can be distinguished. At low  $Z$ ,  $R_H$  is  $30\text{--}40 \text{ \AA}$  within the temperature range applied in this study, which is consistent with that of a single

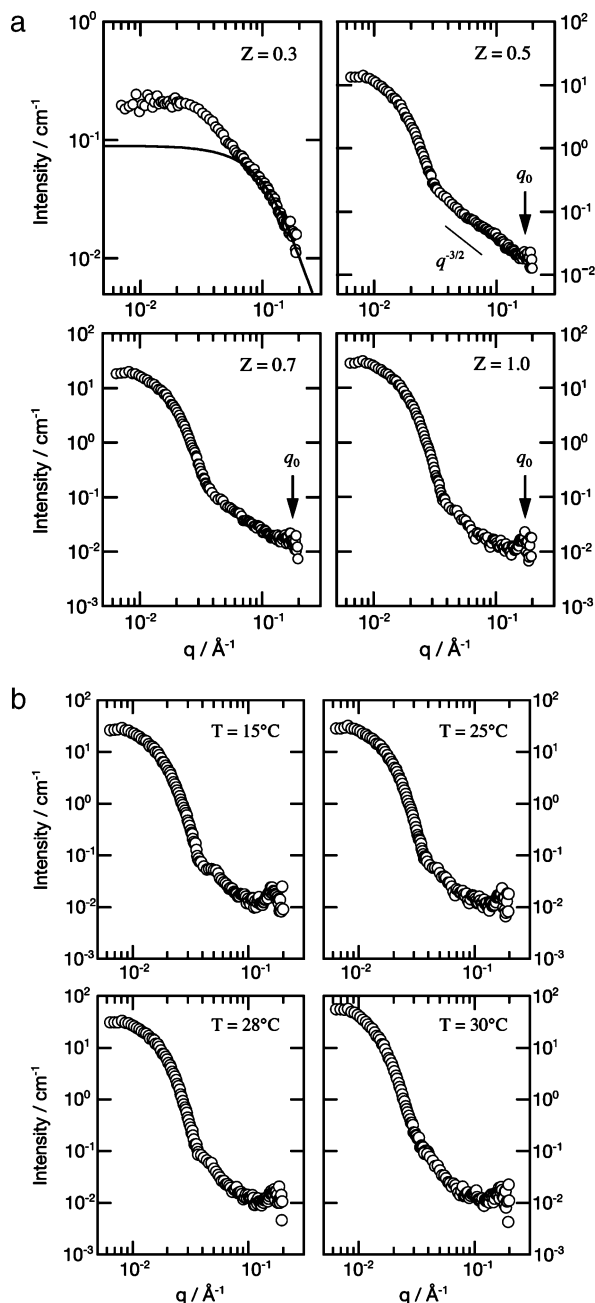


**Figure 7.** (a) SANS profiles for a 0.4 wt % aqueous solutions of  $N_{135}A_{45}/DTAB$  with different charge ratio  $Z$  at 25 °C. The arrow indicates the position of the structure peak at  $q_0 \approx 0.16 \text{ \AA}^{-1}$ . The solid line represents the form factor of polydisperse and homogeneous DTAB micelles of average radius  $R_{Mic} = 19 \text{ \AA}$ . (b) SANS profiles for a 0.4 wt % aqueous solution of  $N_{135}A_{45}/DTAB$  with charge ratio  $Z = 1$  at different temperatures.

block copolymer. Above  $Z_C$ , we observe a sharp increase in hydrodynamic radius that is rather constant in  $Z$  around 200 Å below 30 °C, and 250 Å at 30 °C. The hydrodynamic radius becomes larger with temperature, which reflects the fact that the contraction of the PNIPAM corona of the colloidal complexes starts to occur due to dehydration of the chains, and the complexes form aggregates to avoid contact with water.

**Microstructure of the Colloidal Complex.** Figure 7a compares the scattering cross sections of the colloidal complexes obtained by SANS for 0.4 wt % aqueous solutions of  $N_{135}A_{45}/DTAB$  with different charge ratio  $Z$  at 25 °C. Figure 7b displays the scattering cross sections for a 0.4 wt % aqueous solution of  $N_{135}A_{45}/DTAB$  with charge ratio  $Z = 1$  at different temperatures.

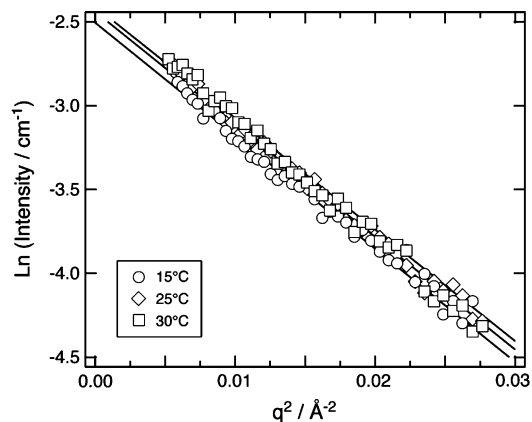


**Figure 8.** Guinier representation of the SANS data obtained from a 0.4 wt % aqueous solution of  $N_{135}A_{45}/DTAB$  with  $Z = 0.3$  at different temperatures.

**TABLE 3: List of the Parameters Obtained from the Guinier Analysis of the SANS Data at  $c = 0.4 \text{ wt \%}$  and  $Z = 0.3$**

	temp = 15 °C	temp = 25 °C	temp = 28 °C	temp = 30 °C
$R_g/\text{\AA}$	$14.5 \pm 2.0$	$14.3 \pm 1.9$	$14.6 \pm 2.0$	$14.7 \pm 2.1$
$R_{Mic}/\text{\AA}$	18.7	18.9	18.8	18.9

The scattering cross section is dominated by a strong forward scattering and by the appearance of a structure peak at high wavevectors. This peak is located around  $q_0 = 0.16 \text{ \AA}^{-1}$ . The amplitude of this peak depends on charge ratio  $Z$ . For  $Z \geq 0.7$ , it dominates the high  $q$ -region. It is worthy to mention that for  $Z = 1$  there is a damped oscillation in the intensity decay around  $0.05 \text{ \AA}^{-1}$ . Berret and co-workers reported that these features are correlated, and they are characteristic to the core-shell aggregates.<sup>11</sup> For  $Z \leq 0.5$ , the peak becomes a weak bump, which seems to be superimposed to a power law dependence of the form  $I(q) \approx q^{-3/2}$ . In copolymer micelles, the contribution of the corona manifests itself at a high wavevector as a power law of the form  $I(q) \approx q^{-1/\nu}$ , where  $\nu$  is the Flory exponent. For Gaussian chains  $\nu = 1/2$ , which gives a  $q^{-2}$  decrease of the intensity, whereas for chains in good solvent  $\nu = 3/5$  and intensity decreases as  $q^{-5/3}$ . Scaling exponents of the order of  $-3/2$  are close to those for polymers in good solvent. This critical  $Z$  value is consistent with that observed by DLS.

The solid line in Figure 7a ( $Z = 0.3 < Z_C$ ) is calculated by using a form factor of polydisperse and homogeneous spheres of average radius  $R = 19 \text{ \AA}$  (standard deviation,  $\sigma_R = 2.5 \text{ \AA}$ ). In the  $q$ -region of  $0.07 \text{ \AA}^{-1} < q < 0.17 \text{ \AA}^{-1}$ , therefore, we could assume that polymer chains do not contribute to the scattering intensity. The SANS data for  $Z = 0.3$  are plotted in Figure 8 by using the Guinier representation for spherical particles as a function of temperature. Here we consider the data only at high  $q$ -region ( $0.07 \text{ \AA}^{-1} < q < 0.17 \text{ \AA}^{-1}$ ). All the data exhibit an exponential decrease of the intensity against  $q^2$ . The straight lines result from the best-fit calculations, using the expression

$$I(q) = I(q=0) \exp\left(-\frac{R_g^2 q^2}{3}\right) \quad (4)$$

where  $I(q=0)$  is the intensity extrapolated at zero wavevector and  $R_g$  is the radius of gyration of the particles. These two quantities are adjustable parameters in the fitting. In Table 3,

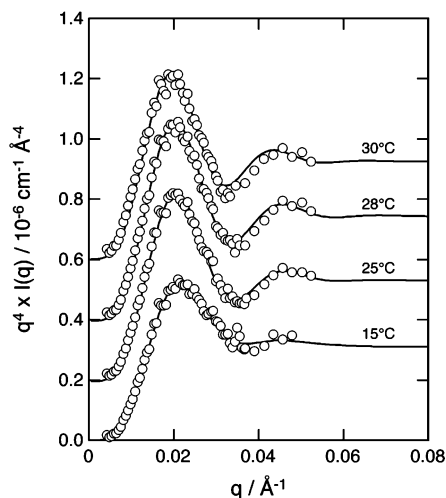


**Figure 9.** Porod representation of the SANS intensity for a 0.4 wt % aqueous solution of  $N_{135}A_{45}/DTAB$  with  $Z = 0.7$  at different temperatures. For clarity the data are shifted by additive factors  $2 \times 10^{-7}$  (25 °C),  $4 \times 10^{-7}$  (28 °C), and  $6 \times 10^{-7}$  (30 °C) with respect to the data at 15 °C.

the parameters obtained from Guinier analysis are listed. For  $Z = 0.3$ , below 15 °C, the radius of gyration is about  $14.5 \pm 2.0$  Å, which corresponds to an actual micelle radius,  $R_{Mic}$ , of 19 Å via  $R_{Mic} = \sqrt{5/3}R_g$  assuming homogeneous particles.<sup>19</sup> The radius of gyration for pure DTAB ( $Z = \infty$ ) is reported to be  $\sim 17$  Å.<sup>20</sup> These results suggest that the particles detected by SANS are spherical DTAB micelles decorated by one or several PNIPAM-*b*-PAA chains through electrostatic interaction. The radius of gyration  $R_g$  of the particle decreases with increasing temperature, which is due to the dehydration of corona PNIPAM chains of the particles. The observed behaviors are identical with those obtained for  $Z = 0.5$ . It is worthy to mention that SANS experiments indicated the existence of spherical DTAB micelles despite the fact that the surfactant concentration  $c_s$  is below the cmc of DTAB for  $Z = 0.3$ .  $c_s$  is  $2.36 \times 10^{-3}$  ( $Z = 0.3$ ), which is about 5 times lower than the cmc of DTAB (0.46 wt % at ambient temperature). In the  $N_{135}A_{45}/DTAB$  system, most of the bromide counterions of DTAB are replaced by PAA blocks. Since the SANS experiments clearly identify spherical micelle below the cmc, the polymer–surfactant solution is above the critical aggregation concentration (cac).

The SANS intensity at intermediate and low  $q$ -region has been interpreted as arising from spherical and homogeneous particles. To determine the core size of the colloidal complexes formed by the system  $N_{135}A_{45}/DTAB$  at  $Z_C < Z$ , the SANS curves are fitted assuming a Gaussian distribution of homogeneous spheres with an average core radius  $R_C$  and a standard deviation  $\sigma_R$ .<sup>10</sup> At sufficiently low  $c$ , the intermicelle interactions are negligible, therefore the structure factor in eq 3 is 1,  $S(q,c) = 1$ . For homogeneous spheres,  $F(q,R) = [3(\sin X - X \cos X)/X^3]^2$ , where  $X = qR$ . In this regime, for micelles distributed

according to a Gaussian distribution function, the scattering cross section becomes

$$\frac{d\sigma}{d\Omega}(q,c) = n(c)\Delta\rho^2 \int_0^\infty V^2 G(R,R_C,\sigma_R) F(q,R) dR \quad (5)$$

$$G(R,R_C,\sigma_R) = \frac{1}{\sigma_R\sqrt{2\pi}} \exp\left[-\left(\frac{(R-R_C)^2}{2\sigma_R^2}\right)\right] \quad (6)$$

where  $R_C$  and  $\sigma_R$  are the average core radius and standard deviation of the Gaussian function. The data for the  $N_{135}A_{45}/DTAB$  system at  $c = 0.4$  wt % and  $Z = 0.7$  are shown in Figure 9, using the Porod representation. The sample exhibits damped oscillation by fitting assuming a distribution of spherical and homogeneous particles with average radius  $R_C$  and a standard deviation  $\sigma_R$ . The values for  $R_C$  at  $Z = 0.5, 0.7$ , and 1 are summarized in Table 4 for temperature ranging from 15 to 30 °C. Below 30 °C, the average core radius  $R_C$  is comprised between 150 and 160 Å. In this range of charge ratios and temperatures,  $\sigma_R$  remains constant, about 30 Å. The  $R_C$  has values ranging from the micellar radius ( $R_{Mic} \approx 20$  Å) and the hydrodynamic radius ( $R_H \approx 300$  Å). This result is due to the fact that the  $N_{135}A_{45}/DTAB$  forms a core–shell structure. The core dominates the SANS cross section at intermediate wavevector ( $0.01 \text{ Å}^{-1} < q < 0.1 \text{ Å}^{-1}$ ), whereas the corona, which is composed by the PNIPAM blocks, is associated with the hydrodynamic size of the colloidal complex.<sup>20</sup> At 30 °C, the average core radius  $R_C$  increases to  $\sim 170$  Å. Around 30 °C, the PNIPAM corona chains start to collapse due to the dehydration of the chains. The collapsed part of PNIPAM corona chains is likely to locate on the surface of the core and is detected as part of the core by SANS.

We evaluate the aggregation number of micelles  $N_{agg}$  per colloidal complex in the line with the arguments made by Berret and co-workers.<sup>10,20</sup>  $N_{agg}$  can be written:

$$N_{agg} = \phi_{Mic} \left(\frac{R_C}{R_{Mic}}\right)^3 \quad (7)$$

where  $\phi_{Mic}$  is the micellar volume fraction in the core.  $\phi_{Mic}$  is related to the homopolyelectrolyte/surfactant system. Poly-(sodium acrylate) and DTAB in solutions undergo a phase separation, giving rise to a solid precipitate that displays the scattering features of a cubic phase of micelles. The sequence of Bragg peaks is interpreted as arising from a cubic structure associated with the space group of symmetry  $Pm\bar{3}n$ ,<sup>12,21–26</sup> meaning 8 micelles per unit cell and a capacity of 0.524. Since the core of the colloidal complex does not form any crystal structure, we can conclude that the upper limit of the volume fraction of micelle in the core must be less than 0.524. Here we implicitly assume that the mechanism of formation of the colloidal complexes is similar to that driving phase separation, and thus take  $\phi_{Mic} = 0.5$  and  $R_{Mic} = 20$  Å. Values for  $N_{agg}$  are

**TABLE 4:** List of the Parameters Used in the Fitting of Sans Data at  $c = 0.4$  wt % Assuming a Distribution of Spherical Particles of Radius  $R_C$  and Standard Deviation  $\sigma_R$ <sup>a</sup>

temp/°C	$Z = 0.5$			$Z = 0.7$			$Z = 1.0$		
	$R_C/\text{Å}$	$\sigma_R/\text{Å}$	$N_{agg}$	$R_C/\text{Å}$	$\sigma_R/\text{Å}$	$N_{agg}$	$R_C/\text{Å}$	$\sigma_R/\text{Å}$	$N_{agg}$
15	$152 \pm 1.1$	34	219	$156 \pm 1.1$	29	237	$158 \pm 1.7$	29	246
25	$158 \pm 1.1$	31	246	$155 \pm 1.1$	27	233	$156 \pm 1.0$	28	237
28	$156 \pm 1.3$	30	237	$156 \pm 1.4$	28	237	$157 \pm 1.9$	27	241
30	$173 \pm 2.1$	34	-	$162 \pm 1.1$	29	-	$172 \pm 5.0$	28	-

<sup>a</sup> The average number of micelles per colloidal complex  $N_{agg}$  is calculated with eq 7.

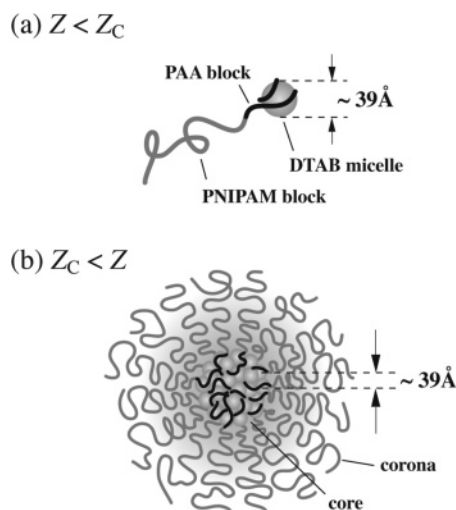


**Figure 10.** Schematic representation of (a) DTA<sup>+</sup> micelle decorated by PNIPAM-*b*-PAA ( $Z < Z_c$ ) and (b) a colloidal complex formed by the association of PNIPAM-*b*-PAA and DTAB ( $Z_c < Z$ ).

given in Table 3 for the series at  $c = 0.7$  wt % depending on  $Z$  and temperature, and they range from 220 to 250.

At large wavevectors ( $0.1 \text{ \AA}^{-1} < q$ ), and charge ratios above the critical value ( $Z_c < Z$ ), the scattering is characterized by a structure peak located around  $q_0 = 0.16 \text{ \AA}^{-1}$ . This peak corresponds to the characteristic distance  $2\pi/q_0 \approx 39 \text{ \AA}$ , and is independent of the charge ratio  $Z$  as well as temperature. The intensity of the peak grows until a stoichiometric PAA block-surfactant complex ( $Z = 1$ ) is formed. This indicates that the stoichiometry of the structural units is not significantly changed, since a charge imbalance would lead to a swelling due to repulsive double-layer force. Therefore, from our observations, the structural picture of the colloidal complex that emerges is that of the core-shell microstructure. By using the analogy with the homopolyelectrolyte/surfactant concentrated phases,<sup>27–30</sup> the core is constituted of densely packed surfactant micelles (DTA<sup>+</sup>), and PAA block chains bind to these micelles, displace their counteranions ( $\text{Br}^-$ ), and bridge them together. The intermicellar distance of the DTA<sup>+</sup> micelles decorated by PAA block chains in the interior is  $\sim 39 \text{ \AA}$ . The outer part of the colloidal complex is corona chains made of thermosensitive PNIPAM chains. On the basis of the SANS results, we propose a schematic representation of the colloidal complex formed by the association of PNIPAM-*b*-PAA and DTAB in Figure 10.

**Salt Effect on Complex Formation.** With addition of surfactant to a polyelectrolyte solution, the surfactant molecules form micelle-like aggregates adsorbed to the polymer chains above a critical surfactant concentration much smaller than the critical micelle concentration of the pure surfactant system. Since the interaction between polyelectrolyte and oppositely charged surfactant is primarily electrostatic in nature, electrostatic factors, such as macromolecular charge densities and ionic strength, are most important factors. Figure 11a shows the distributions of relaxation times of a 0.1 wt %  $\text{N}_{135}\text{A}_{45}/\text{DTAB}$  solution ( $\alpha = 0.75$ ,  $Z = 0.5 < Z_c$ ) at  $q = 1.87 \times 10^{-3} \text{ \AA}^{-1}$  under various NaCl concentrations at 25 °C. At  $[\text{NaCl}] = 0 \text{ M}$ , two relaxation processes are observed. The fast process with diffusivity  $D_{\text{fast}} = 4.7 \times 10^{-7} \text{ cm}^2/\text{s}$ , which corresponds to a hydrodynamic radius  $R_{\text{H,fast}} = 40 \pm 1.2 \text{ \AA}$ , is attributed to single polymer chains, while a slower process with diffusivity  $D_{\text{slow}} = 0.26 \times 10^{-7} \text{ cm}^2/\text{s}$ , which corresponds to a hydrodynamic radius  $R_{\text{H,slow}} = 722 \pm 20 \text{ \AA}$ , is attributed to polymer aggregates including polymer/surfactant complexes. With increasing NaCl concentration, the proportion of the slow process decreases, and almost

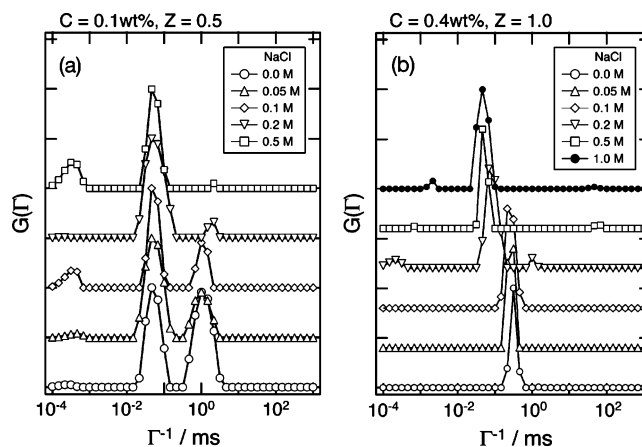


**Figure 11.** (a) The relaxation time distributions for a 0.1 wt %  $\text{N}_{135}\text{A}_{45}/\text{DTAB}$  solution ( $\alpha = 0.75$ ,  $Z = 0.5 < Z_c$ ) at  $q = 1.87 \times 10^{-3} \text{ \AA}^{-1}$  under various NaCl concentrations at 25 °C. (b) The relaxation time distributions for a 0.4 wt %  $\text{N}_{135}\text{A}_{45}/\text{DTAB}$  solution ( $\alpha = 0.75$ ,  $Z = 1.0 > Z_c$ ) at  $q = 1.87 \times 10^{-3} \text{ \AA}^{-1}$  under various NaCl concentrations at 20 °C.

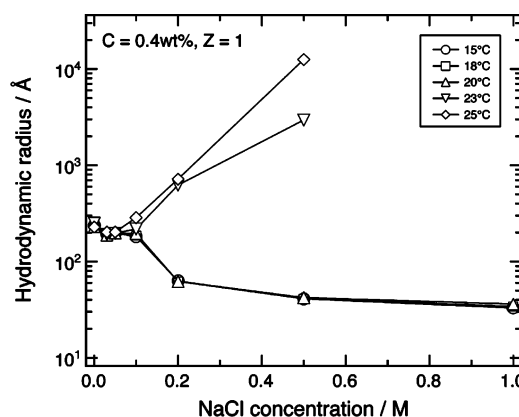


**Figure 12.** The NaCl concentration dependence of the hydrodynamic radius  $R_{\text{H}}$  for a 0.4 wt %  $\text{N}_{135}\text{A}_{45}/\text{DTAB}$  aqueous solution with  $\alpha = 0.75$  and  $Z = 1$  at various temperatures.

disappears at  $[\text{NaCl}] = 0.5 \text{ M}$ . The addition of salt weakens the strength of complex formation; that is, the critical surfactant concentration for the onset of complex formation increases with salt concentration. Furthermore, the addition of excess salt completely suppresses the formation of polymer/surfactant complexes.<sup>31–34</sup> These salt-reducing effects on the complex formation are generally explained in terms of the reduction or complete screening of the electrostatic attraction between polyelectrolyte and surfactant. Figure 11b exhibits the distributions of relaxation times of a 0.4 wt %  $\text{N}_{135}\text{A}_{45}/\text{DTAB}$  solution ( $\alpha = 0.75$ ,  $Z = 0.5 > Z_c$ ) at  $q = 1.87 \times 10^{-3} \text{ \AA}^{-1}$  under various NaCl concentrations at 20 °C. The changes in the hydrodynamic radii for a 0.4 wt %  $\text{N}_{135}\text{A}_{45}/\text{DTAB}$  solution ( $\alpha = 0.75$ ,  $Z = 0.5 > Z_c$ ) at different temperatures are plotted as a function of NaCl concentration in Figure 12. The distribution of the relaxation time exhibits a relatively narrow and unimodal peak, indicating the formation of the colloidal complex is not suppressed within the NaCl concentration range applied here. At  $T \leq 20 \text{ °C}$ , as shown in Figure 12, the hydrodynamic radius gradually decreases with increasing NaCl concentration, which may be attributed to the collapse of PNIPAM corona chains. The change in the dimension of the corona chains by the addition of salt molecules is induced by the change in the interaction between solvent and PNIPAM chains. The observed behavior suggests that the ordered structure in water around the hydrophobic moiety of PNIPAM chains is broken by the addition of



salts, and that the net entropy of the water is affected. The coil-to-globule transition of PNIPAM chains in the aqueous salt solutions is related with the dehydration with respect to hydrophobic hydration. The observed behavior is caused by the increase in entropy of the water by the addition of salts.<sup>35–38</sup> On the other hand, above 20 °C, the hydrodynamic radius gradually increases with increasing NaCl concentration. The coil-to-globule transition temperature of PNIPAM decreases with increasing salt concentrations. The transition temperature in NaCl aqueous solution,  $T_{\text{NaCl}}$ , becomes lower than that in water,  $T_{\text{water}}$ . In addition, the width of the transition, that is the difference in dimension between swollen and collapsed phases at the transition threshold, increased. As NaCl concentration increased, the difference between  $T_{\text{water}}$  and  $T_{\text{NaCl}}$  becomes larger, and the transition width further increased.<sup>35–38</sup> Therefore the increase in the hydrodynamic radius is attributed to the increased fraction of dehydrated PNIPAM corona chains leading to more hydrophobic interactions between the polymer chains and therefore to aggregation of the colloidal complexes. The addition of salt screens the electrostatic attraction between oppositely charged polymer and surfactant, which weakens the interaction. This salt effect can be designated as the screening of interaction. On the other hand, the addition of salt enhances the dehydration of PNIPAM chains. Therefore, in the colloidal complex, PNIPAM corona chains tend to collapse at higher salt concentration and temperature. This salt effect can be designated as the increasing of interaction. Therefore, the overall effect of salt depends on the competition of increasing hydrophobic interaction among PNIPAM coronas with the screening of the electrostatic interaction between PAA blocks and surfactants.

## Conclusion

In this study, the microscopic structure of a colloidal complex comprised of PNIPAM-*b*-PAA and oppositely charged surfactant DTAB in water was investigated by DLS and SANS. PNIPAM-*b*-PAA with low polydispersity was prepared by RAFT polymerization in methanol. DLS and SANS clearly indicate that the aqueous solution of PNIPAM-*b*-PAA and DTAB associates into colloidal complexes. For low surfactant-to-polymer charge ratio  $Z$  lower than the critical value  $Z_c$ , the colloidal complexes are single DTAB micelles dressed by a few PNIPAM-*b*-PAA. Above the critical value  $Z_c$ , the colloidal complexes form a core-shell microstructure. The core of the complex consists of densely packed surfactant micelles ( $\text{DTA}^+$ ), and PAA block chains bind to these micelles, displace their counteranions ( $\text{Br}^-$ ), and bridge them together. The core radius ranges between 150 and 160 Å depending on the charge ratio and temperature, and the intermicellar distance of the  $\text{DTA}^+$  micelles is  $\sim 39$  Å, which is independent of the charge ratio  $Z$  as well as temperature. The corona of the complex is constituted from the thermosensitive PNIPAM. The aggregation number expressed in terms of  $\text{DTA}^+$  micelles per complex is also determined by using the analogy with the homopolyelectrolyte/surfactant system, and found to be 200–250 depending on the charge ratio and temperature.

**Acknowledgment.** The work was partly supported by a Grant-in-Aid (No. 17350060) and a Grant-in-Aid for Scientific Research on Priority Areas “Soft Matter Physics” (No. 19031024) from the Ministry of Education, Culture, Sports, Science, and Technology of Japan. This work was performed with the approval of the Institute for Solid State Physics, The University of Tokyo (Proposal No. 6573).

## References and Notes

- (1) Zhou, S.; Chu, B. *Adv. Mater.* **2000**, *12*, 545.
- (2) Lindman, B.; Thalberg, K. In *Interactions of Surfactants with Polymers and Proteins*; Goddard, E. D., Ananthapadmanabham, K. P., Eds.; CRC Press: Boca Raton FL, 1993.
- (3) Ober, C. K.; Wegner, G. *Adv. Mater.* **1997**, *9*, 17.
- (4) Antonietti, M.; Burger, C.; Thünemann, A. *Trends Polym. Sci.* **1997**, *5*, 262.
- (5) Macknight, W. J.; Ponomarenko, E. A.; Tirrell, D. A. *Acc. Chem. Res.* **1998**, *31*, 781.
- (6) Boronich, T. K.; Kavanov, A. V.; Kabanov, V. A.; Yu, K.; Eisenberg, A. *Macromolecules* **1997**, *30*, 3519.
- (7) Kavanov, A. V.; Boronich, T. K.; Kabanov, V. A.; Yu, K.; Eisenberg, A. *J. Am. Chem. Soc.* **1998**, *120*, 9941.
- (8) Boronich, T. K.; Cherry, T.; Vinogradov, S. V.; Eisenberg, A.; Kavanov, A. V.; Kabanov, V. A. *Langmuir* **1998**, *14*, 6101.
- (9) Lysenko, E. A.; Boronich, T. K.; Eisenberg, A.; Kavanov, V. A.; Kabanov, A. V. *Macromolecules* **1998**, *31*, 4511.
- (10) Hervé, P.; Destarac, M.; Berret, J.-F.; Lal, J.; Oberdisse, J.; Grillo, I. *Europhys. Lett.* **2002**, *58*, 912.
- (11) Berret, J.-F.; Hervé, P.; Aguerre-Chariol, O.; Oberdisse, J. *J. Phys. Chem.* **2003**, *107*, 8111.
- (12) Berret, J.-F.; Vigolo, B.; Eng, R.; Hervé, P.; Grillo, I.; Yang, L. *Macromolecules* **2004**, *37*, 4922.
- (13) Chiefari, J.; Chong, Y. K.; Elcore, F.; Krstina, J.; Jeffery, J.; Le, T. P. T.; Mayadunne, R. T. A.; Meijs, G. F.; Moad, C. L.; Moad, G.; Rizzardo, E.; Thang, S. H. *Macromolecules* **1998**, *31*, 5559.
- (14) Perrier, S.; Barner-Kowollik, C.; Quinn, J. F.; Vana, P.; Davis, T. P. *Macromolecules* **2002**, *35*, 8300.
- (15) Nakayama, M.; Okano, T. *Biomacromolecules* **2005**, *6*, 2320.
- (16) Okabe, S.; Karino, T.; Nagao, M.; Watanabe, S.; Shibayama, M. *Nucl. Instrum. Methods Phys. Res., Sect. A* **2007**, *572*, 853.
- (17) Bales, B. L.; Zana, R. *J. Phys. Chem. B* **2002**, *106*, 1926.
- (18) Berret, J.-F. *J. Chem. Phys.* **2005**, *123*, 164703.
- (19) Büttin, V.; Armes, S. P.; Billingham, N. C.; Tuzar, Z.; Rankin, A.; Eastoe, J.; Heenan, R. K. *Macromolecules* **2001**, *34*, 1503.
- (20) Berret, J.-F.; Cristobal, G.; Hervé, P.; Oberdisse, J.; Grillo, I. *Eur. Phys. J. E* **2002**, *9*, 301.
- (21) Sokolov, E.; Yeh, F.; Khokhlov, A.; Grinberg, V. Y.; Chu, B.; *J. Phys. Chem. B* **1998**, *102*, 7091.
- (22) Zhou, S.; Yeh, F.; Burger, C.; Chu, B. *J. Phys. Chem. B* **1999**, *103*, 2107.
- (23) Ashbaugh, H. S.; Lindman, B. M. *Macromolecules* **2001**, *34*, 1522.
- (24) Kogej, K.; Evmenenko, G.; Theunissen, E.; Berghmans, H.; Reynaers, H. *Langmuir* **2001**, *17*, 3175.
- (25) Svensson, A.; Topgaard, D.; Piculell, L.; Söderman, O. *J. Phys. Chem. B* **2003**, *107*, 13241.
- (26) Seddon, J. M.; Robins, J.; Gulick-Krywicki, T.; Delacroix, H. *Phys. Chem. Chem. Phys.* **2000**, *2*, 4485.
- (27) Iekti, P.; Piculell, L.; Tournilhac, F.; Cabene, B. *J. Phys. Chem. B* **1998**, *102*, 344.
- (28) Iekti, P.; Martin, T.; Cabene, B.; Piculell, L. *J. Phys. Chem. B* **1999**, *103*, 9831.
- (29) Svensson, A.; Piculell, L.; Iekti, P.; Cabene, B. *J. Phys. Chem. B* **2002**, *106*, 1013.
- (30) Claesson, P. M.; Bergström, M.; Dedinaite, A.; Kjellin, M.; Legrand, J.-F.; Grillo, I. *J. Phys. Chem. B* **2000**, *104*, 11689.
- (31) Thalberg, K.; Lindman, B. *J. Phys. Chem.* **1989**, *93*, 1478.
- (32) Herslöf-Björling, Å.; Björling, M.; Sundelöf, L. *Langmuir* **1999**, *15*, 353.
- (33) Thalberg, K.; Lindman, B.; Bergfeldt, K. *Langmuir* **1991**, *7*, 2893.
- (34) Villetti, M. A.; Borsali, R.; Crespo, J. S.; Soldi, V.; Fukuda, K. *Macromol. Chem. Phys.* **2004**, *205*, 907.
- (35) Suzuki, A. *Adv. Polym. Sci.* **1993**, *110*, 226.
- (36) Sasaki, S.; Kawasaki, H.; Maeda, H. *Macromolecules* **1997**, *30*, 1847.
- (37) Annaka, M.; Motokawa, K.; Sasaki, S.; Nakahira, T.; Kawasaki, H.; Maeda, H.; Amo, Y.; Tomonaga, Y. *J. Chem. Phys.* **2000**, *113*, 5980.
- (38) Annaka, M.; Amo, Y.; Sasaki, S.; Tomonaga, Y.; Motokawa, K.; Nakahira, T. *Phys. Rev. E* **2002**, *65*, 031805.